Observation of ultrafast spin-lattice relaxation in Tm^{2+}-doped CaF_2 and SrF_2 crystals by optical means

Kohmoto, Toshiro

Fukuda, Yukio

Kunitomo, M.

Isoda, K.

(Citation)
Physical Review B,62(1):579-583

(Issue Date)
2000-07

(Resource Type)
journal article

(Version)
Version of Record

(URL)
https://hdl.handle.net/20.500.14094/90000237

Observation of ultrafast spin-lattice relaxation in Tm^{2+}-doped CaF_2 and SrF_2 crystals by optical means

T. Kohmoto, Y. Fukuda, and M. Kunitomo
Department of Physics, Faculty of Science, Kobe University, Nada, Kobe 657-8501, Japan

K. Isoda
Graduate School of Science and Technology, Kobe University, Nada, Kobe 657-8501, Japan
(Received 27 December 1999)

Ultrafast spin-lattice relaxation in the ground state of Tm^{2+} doped in CaF_2 and SrF_2 crystals is studied. The magnetization is created and detected by optical pulses, and spin-lattice relaxation times of the order of picoseconds or femtoseconds, which cannot be measured by the conventional electron spin resonance, can be obtained from the decay curves of the magnetization. It was found that the temperature dependences of the spin-lattice relaxation rate $1/T_1$ near room temperature are deviated from the T^9 dependence, which is expected from the well-known Raman process of phonons. Considering the effect of the Debye temperature θ_D of the host crystal on the Raman process, the observed temperature dependences of $1/T_1$ are explained consistently both for Tm^{2+}:CaF_2 (θ_D=513 K) and Tm^{2+}:SrF_2 (θ_D=378 K).

I. INTRODUCTION

The divalent thulium ion Tm^{2+} in alkaline-earth fluoride hosts, CaF_2,SrF_2, and BaF_2, has attractive properties. In these host crystals, this ion is in a cubic field and has strong absorption bands in the visible region with large paramagnetic circular dichroism.[1,2] Many interesting studies by optical means have been reported on Tm^{2+} ion in cubic fields, such as spin-orientation memory,[3,4] enhancement of nuclear polarization,[5,6] spin-phonon interactions,[7] electron spin resonance (ESR) in the metastable state,[3,8] ESR free-induction decay,[9] and spin cross relaxation.[10,11]

In the study on fast spin dynamics in condensed matter near room temperature, optical pumping with a short laser pulse is very useful. The observation of the spin relaxation[12,13] and the free-induction-decay signal[14] in nanosecond region have been reported, where the time evolution of the optically induced magnetization was monitored by a pickup coil. However, the resolution time of the detection system in such experiments is of the order of 1 ns. If the induced magnetization can be monitored by an optical pulse, the time resolution can be remarkably improved, and the ultrafast spin dynamics in picosecond or femtosecond region can be observed. Such studies on the ultrafast spin dynamics have been reported in dilute magnetic semiconductors[15,16] and metals.[17,18]

In the present paper we report on the observation of ultrafast spin-lattice relaxation in the ground state of Tm^{2+} in CaF_2 and SrF_2 near room temperature. The magnetization is created by an optical pump pulse, and spin-lattice relaxation times of the order of picoseconds or femtoseconds can be obtained from the decay curves of the magnetization. Such ultrashort relaxation times cannot be measured by the conventional ESR, whose time resolution is nanoseconds at best. The time resolution of our optical method is limited only by the temporal width of the light pulses, and investigation of ultrafast spin dynamics can be realized.

In the experiment, the pump-probe technique is used to observe the spin-lattice relaxation in the ground state of the divalent thulium ion (Tm^{2+}) doped in CaF_2 and SrF_2 crystals. The magnetic circular dichroism (MCD) of the optical transition is responsible for the creation and the detection of the magnetization. Absorption and MCD spectra for Tm^{2+}:SrF_2 are shown in Fig. 1.[19] Those for Tm^{2+}:CaF_2 are similar to the spectra in Fig. 1.[2] The magnetization is instantaneously created in the ground state by a circularly polarized pump pulse. The created magnetization is monitored as the change of the polarization of a linearly polarized probe pulse. Decay curve of the magnetization is measured by changing the optical delay between the pump and probe pulses, and the spin-lattice relaxation time T_1 is obtained from the decay curve.

The value of T_1, which is of the order of seconds at liquid-helium temperatures, becomes of the order of picoseconds near room temperature. The spin-lattice relaxation in the higher temperature region is caused by the Raman pro-

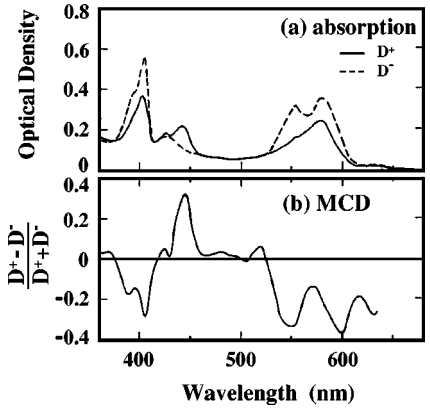

FIG. 1. (a) Absorption and (b) magnetic circular dichroism (MCD) spectra of Tm^{2+}:SrF_2 obtained by extrapolation to $\mu_B H/kT \rightarrow \infty$ (Ref. 19). D^+ in (a) refers to absorption for σ^+ light and D^- refers to σ^-. The fractional change is shown in (b).

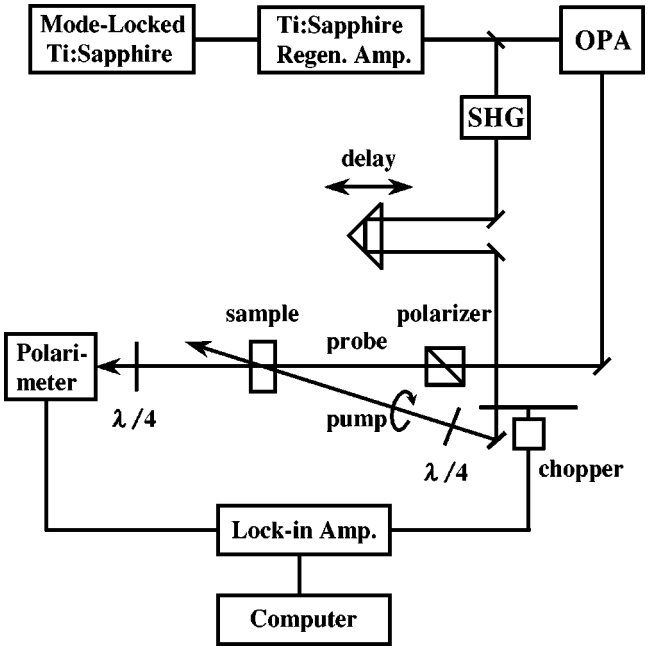

FIG. 2. Experimental setup for the measurement of ultrashort spin-lattice relaxation times. SHG; second harmonic generator, OPA; optical parametric amplifier.

cess of phonons, where the temperature dependence of the relaxation rate for the Kramers ion is expected as $1/T_1 \propto T^9$. The values of $1/T_1$ obtained in our experiment, however, are deviated from this T^9 dependence. To explain the experimental data, we consider a theory of the Raman process which is based on the Debye model of the lattice vibration. Using this theory the observed temperature dependences of $1/T_1$ are explained consistently both for Tm^{2+}:CaF_2 and Tm^{2+}:SrF_2.

II. EXPERIMENT

The experimental setup for the measurement of spin-lattice relaxation times is shown in Fig. 2. The pump pulse is provided by the second harmonics (SH) of a Ti:sapphire regenerative amplifier and the probe pulse by a optical parametric amplifier (OPA). The wavelength is 400 nm for the pump pulse and 560 nm for the probe pulse. The circularly polarized pump beam and the linearly polarized probe beam are nearly collinear and focused on the sample in a refrigerator. The waist size of the beams at the sample are about 100 μm. The pulse energy and the pulse width at the sample are $\sim$10 μJ and 0.2 ps for the pump pulse and $\sim$1 μJ and 0.2 ps for the probe pulse.

Because of the selection rules of the optical transition, population differences (or magnetization) in the magnetic sublevels of the ground state, whose electron spin is 1/2, are instantaneously created by the circularly polarized pump pulse. The created magnetization is detected by a quarter-wave plate and a polarimeter as the change of the polarization of the linearly polarized probe pulse.

The construction of the polarimeter is shown in Fig. 3. The polarimeter[8,20] detects the rotation of polarization plane of a light beam. A linearly polarized beam is split by a Glan prism and incident on the two photodiodes whose photocurrents are subtracted at a resistor. When the Glan prism is mounted at an angle of 45° to the plane of polarization of the light beam, the two photocurrents cancel. If the plane of polarization rotates, the two currents do not cancel and the voltage appears at the resistor.

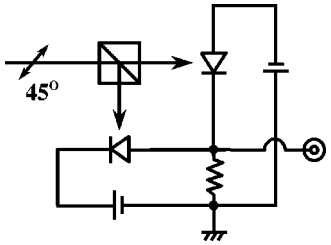

FIG. 3. Construction of the polarimeter.

In the present experiment, the magnetization in the ground state is created by the pump pulse, and then the circular dichroism of the optical transition is induced in the sample. The linearly polarized probe beam is considered to be a superposition of two circularly polarized components which have the opposite polarizations and the same intensities. The induced circular dichroism destroys the intensity balance between the two components. The two circularly polarized beams are transformed by the quarter-wave plate to two linearly polarized beams whose polarizations are crossed each other, and the unbalance of circular polarization is transformed to the unbalance of linear polarization or the rotation of polarization plane. This rotation is detected by the polarimeter as the signal of the magnetization in the ground state.

The time evolution of the magnetization was observed by changing the optical delay between the pump and probe pulses. The spin-lattice relaxation time was obtained from the decay curve of the magnetization. A chopper (180 Hz) for the pump beam and a lock-in amplifier were used to improve the signal-to-noise ratio. For long relaxation times ($>$100 ns) at lower temperatures, the decay curve of the magnetization was monitored by a cw probe light of 610 nm from a dye laser, instead of the probe pulse, and the spin-lattice relaxation time was obtained from the wave form digitized on an oscilloscope.

In the experiment a magnetic field of 200 Oe is applied parallel to the laser beams. In no external magnetic field, the optically created magnetization is destroyed in the time region of $\sim$10 ns by the inhomogeneous local field,[9] which is due to the superhyperfine interaction between the Tm^{2+} ion and neighboring F nuclei and whose direction is randomly distributed. In an external field parallel to the pump beam, whose magnitude is more than that of the local field ($\sim$10 Oe), the decay due to the superhyperfine interaction is suppressed and the created magnetization is held along the external field. The spin-lattice relaxation time due to the direct process of phonons depends on the magnetic field.[21] However, that, due to the Raman process, is independent of the magnetic field.

III. EXPERIMENTAL RESULTS

Decay curves of the magnetization in the ground state of Tm^{2+}:CaF_2 (0.02%Tm^{2+}, 2 mm in thickness, Optovac Inc.) at 140, 210, and 298 K (room temperature) are shown in Fig.

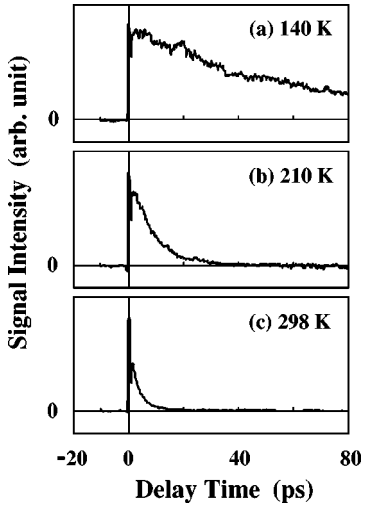

FIG. 4. Decay curves of the magnetization in Tm^{2+}:CaF_2 at (a) 140 K, (b) 210 K, and (c) 298 K. The obtained spin-lattice relaxation times are 60, 10, and 5 ps, respectively.

4. The decay curve of the magnetization is fitted well to a single exponential. The obtained spin-lattice relaxation times are 60, 10, and 5 ps for 140, 210, and 298 K, respectively.

The estimated spin number from the absorbed photon number and the magnitude of MCD at 400 nm, which contributes to the magnetization created at $t=0$ by the pump pulse, is $\sim 10^{12}$ spins in the focused region. This value corresponds to spin density of $\sim 10^{17}$spins/cm^3.

Temperature dependence of the spin-lattice relaxation rate $1/T_1$ in the ground state of Tm^{2+}:CaF_2 is shown in Fig. 5. The data at the lower temperatures are those which have been obtained from the experiment of the electron spin resonance (ESR),[21] where the spin-lattice relaxation is explained by the direct process and the Raman process of phonons. The value of T_1 ranges from seconds at liquid-helium temperatures to picoseconds near room temperature. Thus, in this sample, the spin-lattice relaxation times varying over 11 orders of magnitude can be observed by using the present optical method. The spin-lattice relaxation at the higher temperatures is caused by the Raman process of phonons, and

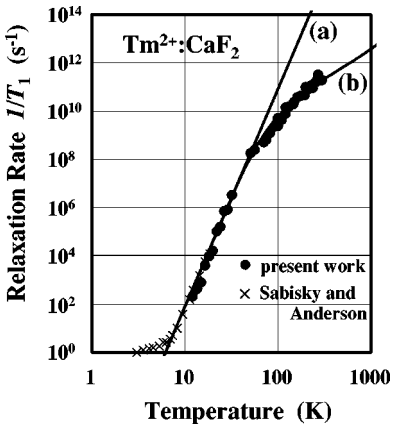

FIG. 5. Temperature dependence of the spin-lattice relaxation rate $1/T_1$ for Tm^{2+}:CaF_2. Solid circle; present work, $\times$; Sabisky and Anderson (Ref. 21). The solid lines are obtained (a) from Eq. (1) and (b) from Eq. (5).

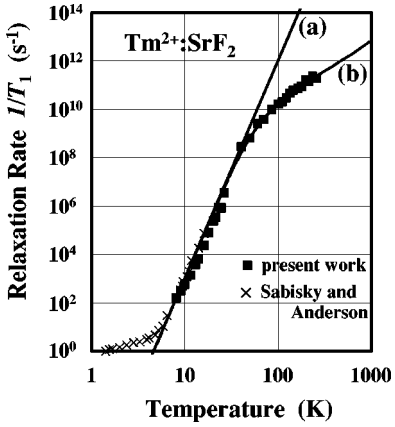

FIG. 6. Temperature dependence of the spin-lattice relaxation rate $1/T_1$ for Tm^{2+}:SrF_2. Solid square; present work, $\times$; Sabisky and Anderson (Ref. 21). The solid lines are obtained (a) from Eq. (1) and (b) from Eq. (5).

the temperature dependence of the relaxation rate for the Kramers ion is expected as $1/T_1 \propto T^9$, which is shown by the straight line (a) in Fig. 5. The values of $1/T_1$ obtained in our experiment at higher temperatures, however, deviate from this T^9 dependence.

To compare the spin-lattice relaxations in different host crystals, we also measured the spin-lattice relaxation times in Tm^{2+}:SrF_2. The optical and magnetic properties of Tm^{2+}:SrF_2 are similar to those of Tm^{2+}:CaF_2,[2,7] and the experimental condition is the same as that in the case of Tm^{2+}:CaF_2. Temperature dependence of the spin-lattice relaxation rate $1/T_1$ in the ground state of Tm^{2+}:SrF_2 (0.02%Tm^{2+}, 1 mm in thickness, Optovac Inc.) is shown in Fig. 6. The data at the lower temperatures are those which have been obtained from the experiment of the ESR.[21] The values of the spin-lattice relaxation rate at the higher temperatures also deviate from the T^9 dependence, which is shown by the straight line (a) in Fig. 6, as in the case of Tm^{2+}:CaF_2.

IV. DISCUSSION

In the study by the ESR, the spin-lattice relaxation at higher temperatures has been explained by the Raman process of phonons. In the Raman process, the population distribution in the magnetic sublevels of the ground state is changed by a process with a phonon pair. One phonon is absorbed and induces the transition from one of the ground state to a virtual state, and at the same time the other phonon is emitted and induces another transition from the virtual state to the other of the ground state. Any two phonons can take part if their frequency difference is equal to the resonance frequency of the magnetic system, and then the Raman process becomes dominant at higher temperatures where many thermal phonons exist. The spin-lattice relaxation rate due to the Raman process for the Kramers ion has been fitted to the equation

$$\frac{1}{T_1} = AT^9, \tag{1}$$

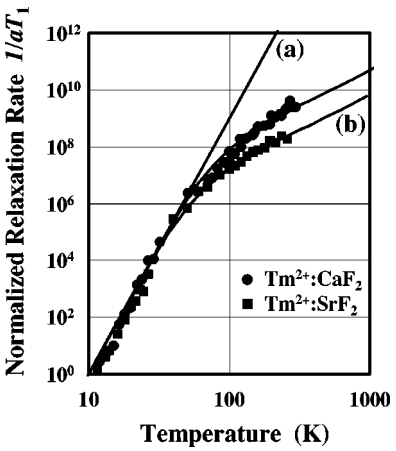

FIG. 7. Temperature dependence of the spin-lattice relaxation rate $1/aT_1$ normalized by the rate at 10 K [Eq. (4)] for Tm^{2+}:CaF_2 (solid circle) and Tm^{2+}:SrF_2 (solid square).

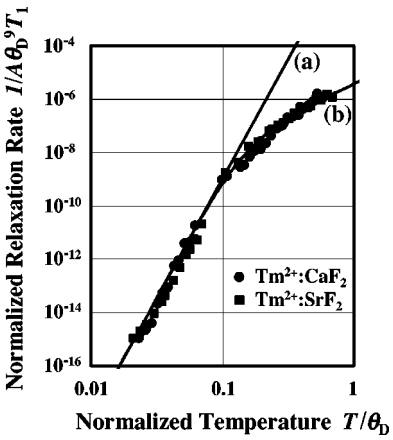

FIG. 8. Normalized spin-lattice relaxation rate $1/A\theta_D{}^9T_1$ [Eq. (7)] for Tm^{2+}:CaF_2 (solid circle) and Tm^{2+}:SrF_2 (solid square). The horizontal axis is the temperature normalized by the Debye temperature T/θ_D.

and the values of the coefficient A have been determined for Tm^{2+} both in CaF_2 and SrF_2;[21]

$$A(\mathrm{CaF_2}) = 7.6\times 10^{-8}\,\mathrm{s^{-1}\,K^{-9}},$$

$$A(\mathrm{SrF_2}) = 1.0\times 10^{-6}\,\mathrm{s^{-1}\,K^{-9}}. \tag{2}$$

The straight lines in Figs. 5 and 6 are obtained from Eq. (1) with Eqs. (2).

In our experiment at the higher temperatures, the values of the spin-lattice relaxation rate deviate from the T^9 dependence both for Tm^{2+}:CaF_2 and Tm^{2+}:SrF_2. Here, to explain these experimental results, we consider the Debye model of the lattice vibration. Turning back to the beginning of the theory of the Raman process, the relaxation rate due to the Raman process for the Kramers ion is expressed as[22]

$$\frac{1}{T_1} = K\int_0^{\omega_m} \frac{\omega^8 \exp(\hbar\omega/kT)}{\{\exp(\hbar\omega/kT)-1\}^2}\,d\omega = K\left(\frac{kT}{\hbar}\right)^9 \int_0^{\theta_D/T} \frac{x^8 e^x}{(e^x-1)^2}\,dx, \tag{3}$$

where K is a constant determined by the interaction between the magnetic ions and the lattice vibrations, $\hbar$ is the Planck constant divided by 2π, k is the Boltzmann constant, ω is the phonon frequency, and ω_m is the maximum phonon frequency corresponding to the Debye temperature θ_D ($\hbar\omega_m = k\theta_D$). Equation (3) means that the rate of the Raman process is due to the phonons with frequencies below ω_m.

In the case of low temperatures ($T \ll \theta_D$), the upper limit θ_D/T of the integral in Eq. (3) can be regarded as infinity, and the integral becomes a constant. Then the well-known expression in Eq. (1) is derived from Eq. (3). In most of the conventional ESR studies on the relaxation, $T \ll \theta_D$ is a good approximation, and Eq. (1) is valid for the relaxation analysis.

Figure 7 shows the temperature dependences of normalized spin-lattice relaxation rate $1/aT_1$, where the rate is normalized by the value of $1/T_1$ at 10 K for each sample;

$$\frac{1}{T_1} = AT^9 = a\left(\frac{T}{10}\right)^9. \tag{4}$$

The straight line (a) shows the normalized rate obtained from Eq. (4) with Eqs. (2). In the lower temperatures, the observed rates for Tm^{2+}:CaF_2 and Tm^{2+}:SrF_2 are on the same line. In the higher temperatures, however, the observed rates for the two samples deviate from the straight line and are separated from each other.

In the case of higher temperatures ($T \geqslant \theta_D$), the integral in Eq. (3) can no longer be regarded as a constant but depends on the temperature. In such a case, as in the case of our experiment, we have to consider the relaxation rate in Eq. (3) taking account of the temperature-dependent integral. Equation (3) can be rewritten as

$$\frac{1}{T_1} = AT^9 f\left(\frac{T}{\theta_D}\right), \tag{5}$$

$$f\left(\frac{T}{\theta_D}\right) = \frac{1}{8!}\int_0^{\theta_D/T} \frac{x^8 e^x}{(e^x-1)^2}\,dx.$$

When $\theta_D/T \to \infty$, the integral approaches 8!, and $f(T/\theta_D) \to 1$. Then Eq. (5) becomes the same with Eq. (1). When $\theta_D/T \to 0$, on the other hand, the integrand approximates to x^6 ($x \ll 0$), and the spin-lattice relaxation rate is expected as $1/T_1 \propto T^2$. The Debye temperatures for CaF_2 and SrF_2 are known as[23,24]

$$\theta_D(\mathrm{CaF_2}) = 513K,$$

$$\theta_D(\mathrm{SrF_2}) = 378K. \tag{6}$$

The curves (b) in Figs. 5, 6, and 7 are obtained from Eq. (5) with Eqs. (2) and (6). It should be noted that there is no new fitting parameter. Our experimental results are explained well by Eq. (5) both for Tm^{2+}:CaF_2 and Tm^{2+}:SrF_2. This shows that the deviation from the T^9 dependence is caused by the finiteness of the phonon frequency.

We also normalize the temperature by the Debye temperature. The normalized equation is given by

$$\frac{1}{A\theta_D{}^9 T_1} = \left(\frac{T}{\theta_D}\right)^9 f\left(\frac{T}{\theta_D}\right). \tag{7}$$

The right side of this equation is a function of T/θ_D, and is expected to exhibit the same behavior for different samples with any different Debye temperatures. Figure 8 shows the normalized spin-lattice relaxation rate $1/A\theta_D{}^9 T_1$ as a function of the normalized temperature T/θ_D. The curve (b) is obtained from Eq. (7), while the straight line (a) is the normalized rate for $f(T/\theta_D)=1$ where the finiteness of the phonon frequency is not taken into account. The observed spin-lattice relaxation rates are on the curve (b) both for Tm^{2+}:CaF_2 and Tm^{2+}:SrF_2. Equation (7) explains our experimental results consistently for the two host crystals. This result shows that the deviation from the T^9 dependence at higher temperatures is due to the lack of high frequency phonons; the distribution of the phonon frequency has the upper limit corresponding to the Debye temperature. It is possible that the Debye temperature of the host crystal is obtained from the temperature dependence of the spin-lattice relaxation rate.

V. SUMMARY

Ultrashort spin-lattice relaxation times in the ground state of Tm^{2+} in CaF_2 and SrF_2 were measured by a pump-probe polarization spectroscopy. The spin-lattice relaxation time ranging over 11 orders of magnitude, from seconds at liquid-helium temperatures to picoseconds near room temperature, can be measured by the optical method. The observed values of the spin-lattice relaxation rate near room temperature deviate from the well-known T^9 dependence for the Raman process of phonons both for Tm^{2+}:CaF_2 and Tm^{2+}:SrF_2. We considered the Debye model of the lattice vibration, and the experimental results were explained consistently for the two samples by taking account of the effect of the Debye temperature of the host crystal.

ACKNOWLEDGMENTS

This work was supported by a grant in aid for scientific research and JSPS research grant for Future Program.

[1] C.H. Anderson, H.A. Weakliem, and E.S. Sabisky, Phys. Rev. **143**, 223 (1966).
[2] H.A. Weakliem, C.H. Anderson, and E.S. Sabisky, Phys. Rev. B **2**, 4354 (1970).
[3] C.H. Anderson and E.S. Sabisky, Phys. Rev. **178**, 547 (1969).
[4] T. Kohmoto, Y. Fukuda, and T. Hashi, Phys. Rev. B **43**, 2519 (1991).
[5] L.F. Mollenauer, W.B. Grant, and C.D. Jeffries, Phys. Rev. Lett. **20**, 488 (1968).
[6] W.B. Grant, L.F. Mollenauer, and C.D. Jeffries, Phys. Rev. B **4**, 1428 (1971).
[7] C.H. Anderson and E.S. Sabisky, in *Physical Acoustics*, edited by W.P. Mason and R.N. Thurston (Academic, New York, 1971), Vol. VIII, Chap. 1.
[8] T. Kohmoto, Y. Fukuda, and T. Hashi, Phys. Rev. B **34**, 6085 (1986).
[9] T. Kohmoto, Y. Fukuda, T. Tanigawa, T. Mishina, and T. Hashi, Phys. Rev. B **28**, 2869 (1983).
[10] E.B. Aleksandrov and V.S. Zapasskii, Fiz. Tverd. Tela (Leningrad) **20**, 1180 (1978) [Sov. Phys. Solid State **20**, 679 (1978)].
[11] T. Kohmoto, Y. Fukuda, and T. Hashi, Phys. Rev. B **39**, 7236 (1989).
[12] J.P. van der Ziel and N. Bloembergen, Phys. Rev. **138**, A1287 (1965).
[13] Y. Takagi, Opt. Commun. **59**, 122 (1986).
[14] Y. Takagi, Y. Fukuda, and T. Hashi, Opt. Commun. **55**, 115 (1985).
[15] D.D. Awschalom, J.-M. Halbout, S. von Molnar, T. Siegrist, and F. Holtzberg, Phys. Rev. Lett. **55**, 1128 (1985).
[16] R. Akimoto, K. Ando, F. Sasaki, S. Kobayashi, and T. Tani, Phys. Rev. B **57**, 1 (1998).
[17] E. Beaurepaire, J.-C. Merle, A. Daunois, and J.-Y. Bigot, Phys. Rev. Lett. **76**, 4250 (1996).
[18] A.Y. Elezzabi, M.R. Freeman, and M. Johnson, Phys. Rev. Lett. **77**, 3220 (1996).
[19] C.H. Anderson and E.S. Sabisky, in *Physical Acoustics* (Ref. 7), p. 21.
[20] R.V. Jones, Proc. R. Soc. London, Ser. A **349**, 423 (1976).
[21] E.S. Sabisky and C.H. Anderson, Phys. Rev. B **1**, 2028 (1970).
[22] A. Abragam and B. Bleaney, *Electron Paramagnetic Resonance of Transition Ions* (Clarendon, Oxford, 1970), Chap. 10.
[23] D.R. Huffman and M.H. Norwood, Phys. Rev. **117**, 709 (1960).
[24] D. Gerlick, Phys. Rev. **136**, A1366 (1964).